surfaces

MDPI

Article

Density Functional Theory Investigations of Carbon Nanotube Unzipping on Cu(111)

Alexandr Alexeev and Sergey N. Filimonov *

Department of Physics, National Research Tomsk State University, 36 Lenin Ave., 634050 Tomsk, Russia
* Correspondence: filimon@phys.tsu.ru; Tel.: +7-3822-529-651

Abstract: The mechanism of carbon nanotube unzipping on a Cu(111) surface was investigated using density functional theory calculations. Optimized structures of armchair and zigzag carbon nanotubes of various sizes were considered, and their energies were compared to those of corresponding planar graphene nanoribbons. The results demonstrate that the flat configuration on the Cu(111) surface is energetically more favorable than the tubular one. As the nanotube diameter increases, the energy difference between the tubular and flat forms decreases due to the reduction in curvature of the nanotubes. Additionally, the energy gain associated with the transformation from nanotubes to nanoribbons is more significant for the zigzag-type structure than for the armchair-type one, suggesting that zigzag carbon nanotubes open more readily on Cu(111). Hypothetical intermediate states in the nanotube-to-nanoribbon transformation were also explored, providing valuable insights into the mechanism of this process.

Keywords: carbon nanotube; graphene; graphene nanoribbon; copper; DFT

1. Introduction

Graphene is a two-dimensional (2D) material composed of a single layer of carbon atoms arranged in a hexagonal lattice. Its outstanding properties, such as high electron mobility and strength, have attracted extensive research interest [1–5]. Graphene is a promising material for many applications, including electronics, solar cells, energy storage, and water treatment [5–10]. Recently, graphene-based particles detectors have been demonstrated [11–13].

However, the use of large-area graphene layers in digital electronic devices is limited due to their zero band gap. On the contrary, graphene nanoribbons (GNRs) may have a non-zero band gap and can be used for fabricating digital electronic devices, such as field effect transistors [14,15]. Notably, the band gap of GNRs is inversely proportional to their width [16,17], so the properties of graphene-based electronic devices can be tuned by controlling the size of GNRs.

There are different approaches to fabricating graphene. One strategy is to grow 2D carbon structures on substrates, for example, by the chemical vapour deposition (CVD) of organic precursor molecules on transition metal surfaces. Cu(111) is widely used as a substrate for CVD of graphene due to the low solubility of C adatoms in copper [18–21] and the possibility of growing graphene layers with low defect density [22,23]. Another approach is to deposit and decompose fullerenes or carbon nanotubes (CNTs) on a surface. In particular, GNRs can be prepared by unzipping CNTs [24]. Since CNTs can be easily synthesized, for instance, by the arc discharge method [25], this approach is very appealing regarding the fabrication costs of GNRs [26,27]. Moreover, unzipping CNTs with well-defined sizes allows for the control of the width and edge structure of GNRs.

The unzipping of CNTs deposited on a substrate can be promoted by chemical oxidation [28], electrical rupture [29], sonication [30], metal-catalyzed unzipping [31], and cryo-milling [32]. Recently, the fabrication of GNRs by the surface-catalyzed unzipping of single-walled carbon nanotubes (SWCNTs) has been reported [33]. It has been shown

check for updates

Citation: Alexeev, A.; Filimonov, S.N. Density Functional Theory Investigations of Carbon Nanotube Unzipping on Cu(111). *Surfaces* **2024**, *7*, 1052–1059. https://doi.org/10.3390/surfaces7040069

Academic Editor: Gaetano Granozzi

Received: 4 November 2024
Revised: 6 December 2024
Accepted: 8 December 2024
Published: 19 December 2024

that SWCNTs adsorbed on Cu(111) unzip to GNRs upon annealing at 820 K. In contrast, SWCNTs deposited on Au(111) desorbed from the surface at 670 K without structural changes. On Ru(0001), the deposited SWCNTs are converted to irregular carbon structures. The experiments with the copper substrate agree with earlier research [34], showing that unzipping of CNTs can occur without external stimuli such as oxidation or unzipping molecules. The feasibility of breaking C-C bonds in sp2-hybridized carbon structures on transition metal surfaces was also reported for fullerens on Ru(0001) and Cu(111) [35,36].

Despite the simplicity of the surface-catalyzed unzipping of CNTs, the mechanism of this process still needs clarification. In this paper, we use DFT calculations to study the relative stability of armchair (AC) and zigzag (ZZ) types of SWCNTs and GNRs adsorbed on Cu(111). Calculations show that on Cu(111), the planar state of GNR is energetically favorable compared with the tubular form of CNT. The energy difference between the CNT and GNR states decreases with the increasing size of carbon structures. Moreover, this difference is more significant for the ZZ-type C structure than for the AC-type, which can be attributed to the lower formation energy of ZZ-GNR on Cu(111) compared with that of AC-GNR. The hypothetical intermediate states of the transformation of the fully closed CNT to the planar GNR were investigated for various sizes of carbon structures.

2. Methods

DFT calculations were carried out using the Fritz Haber Institute ab initio molecular simulations (FHI-aims) package [37]. The generalized gradient approximation (GGA) was used for the exchange-correlation functional in Perdew–Burke–Ernzerhof (PBE) parametrization [38]. The dispersion interactions were accounted for via the Tkachenko–Scheffler (TS) method [39] with screened Van der Waals (VdW) interactions [40]. Structural relaxations were performed via the Broyden–Fletcher–Goldfarb–Shanno (BFGS) optimization algorithm. Default light basis sets were used for structural optimization, and final total energies were calculated using the default tight basis set. Illustrations of geometries were made with the VESTA package [41].

First, the geometry of the bulk copper structure was optimized. The optimized value of the lattice constant was $a_{Cu} = 3.545$ Å, which is in reasonable agreement with the experimental value of 3.615 Å [42].

For surface calculations, we used the three-layer Cu(111) slab with the bottom layer Cu atoms fixed in their bulk positions. Although thicker slabs are often preferred for enhancing the accuracy of surface calculations [43], the three-layer slab used in our study reproduces the periodicity of the FCC crystal in the (111) direction. Therefore, we believe our calculations reliably capture both qualitative and quantitative trends in the adsorption geometries and energies.

In the adsorption calculations, one SWCNT or GNR per unit cell was placed on the top slab surface. We performed calculations with highly anisotropic rectangular unit cells to minimize the lateral interactions of the adsorbed carbon structures with their periodical images (Figure 1). In the z-direction, the slab images were separated by a vacuum region of 50 Å. K-points sampling with a $1 \times 9 \times 1$ grid was used for calculations.

The nanotube diameter d was varied from 0.3 to 0.7 nm. Accordingly, the width of the planar GNR on Cu(111) ranged from 0.9 to 1.9 nm. Due to the lattice mismatch between Cu(111) and graphene, the GNRs (CNTs) were stretched by 1.76% in the longitudinal (axial) direction. The same structural parameters were used for the freestanding CNTs and GNRs calculations.

The images of all optimized structures obtained in our calculations and the input geometry files in the FHI-aims format, containing detailed information on the atomic coordinates of the relaxed structures, can be found in the SI files.

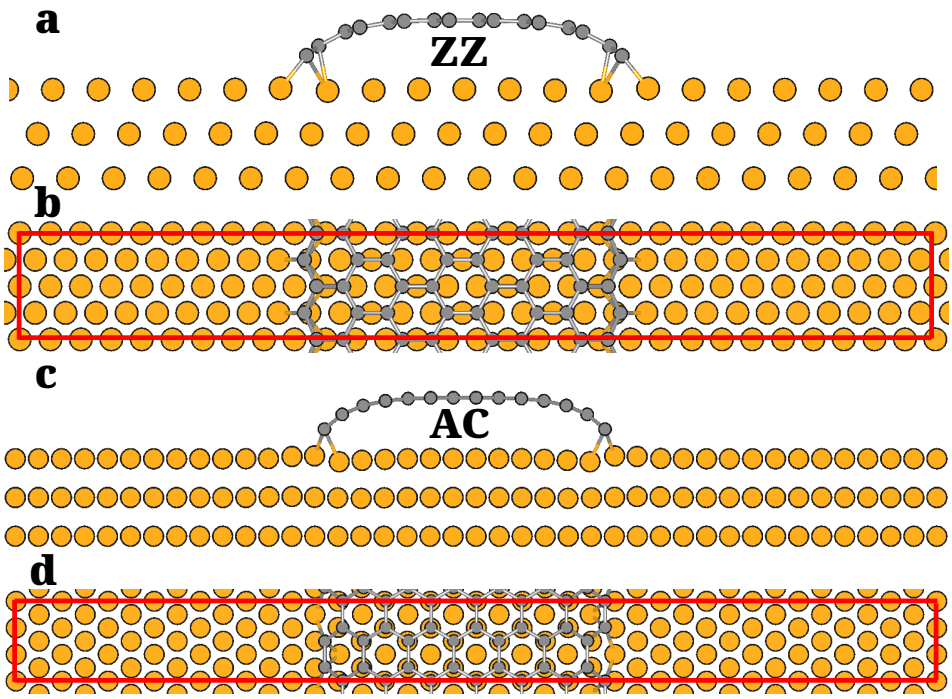

Figure 1. Top and side view of the unit cells used in the calculations of the adsorbed zigzag (**a**,**b**) and armchair (**c**,**d**) graphene nanoribbons.

3. Results and Discussion

To determine the energetically favorable state of the freestanding carbon structures, we calculated the energy difference

$$\Delta E = \frac{1}{N}(E_{CNT} - E_{GNR}), \quad (1)$$

between the total energy of the freestanding carbon nanotube E_{CNT} and the total energy of the fully relaxed freestanding graphene nanoribbon E_{GNR}, normalized to the number of carbon atoms N per calculation unit cell.

As can bee seen from Table 1, for CNTs with a diameter of 0.3–0.4 nm the tubular form is energetically less preferable than the planar one. For large CNTs, the situation is reversed: the total energy of the planar form is lower than that of the tubular form. This behavior can be explained by the decreasing curvature of CNTs with the increasing CNT diameter, which decreases the energy costs due to the bending of the graphitic sp^2 structure and outbalances the energy costs related to the edge formation energy of the GNRs.

Table 1. The energy difference per atom ΔE between the CNT and the GNR carbon forms in the freestanding state. Negative values indicate that freestanding GNRs are energetically unfavorable compared to freestanding CNTs.

d, nm	Type	ΔE, eV
0.3	ZZ	0.26
0.4	AC	0.06
	ZZ	−0.08
0.5	AC	−0.06
	ZZ	−0.16
0.7	AC	−0.11

The optimal configurations of the AC- and ZZ-type CNTs on Cu(111) were identified. Two different states of CNTs on Cu(111) were observed after the structural relaxation of the slab: the optimal (Figure 2a,c) and metastable (Figure 2b,d). For the ZZ-CNT, the metastable state is rotated by 15° around the CNT axis with respect to the optimal state (Figure 2a,b) and by 30° for the AC-CNT (Figure 2c,d). The total energy differences between stable and metastable states of adsorbed CNT are 0.28 eV and 0.11 eV for ZZ and AC type, respectively. In the optimal state, more carbon atoms are bonded with the metal atoms compared to the metastable state.

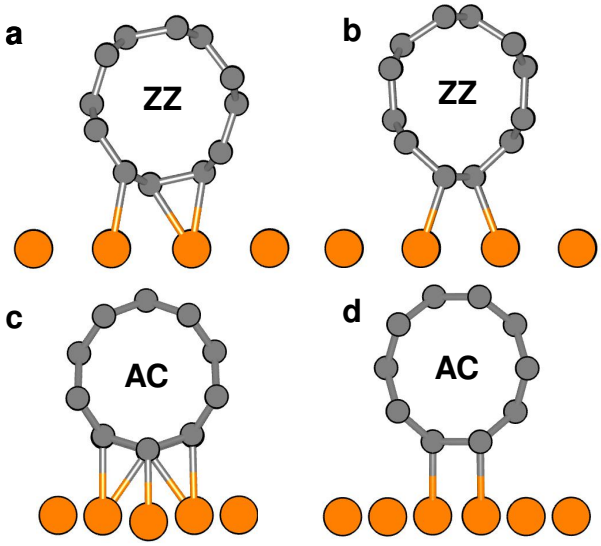

Figure 2. Relaxed geometries of ZZ-CNTs (**top**) and AC-CNTs (**bottom**) in the optimal (**a**,**c**) and metastable (**b**,**d**) orientations on Cu(111).

To characterize the relative stability of the adsorbed carbon structures on Cu(111), we calculated the adsorption energy E_{ad} using the energy of the freestanding CNT E_{CNT} and the energy of the metal slab without the adsorbate $E_{Cu(111)}$ as a reference:

$$E_{ad} = \frac{1}{N}(E_{C+Cu(111)} - E_{CNT} - E_{Cu}). \quad (2)$$

Here, $E_{C+Cu(111)}$ is the total energy of the Cu(111) slab with a carbon structure adsorbed on the top slab surface. The calculated adsorption energies are collected in Table 2.

The tubular form of ZZ-CNT with $d = 0.3$ nm adsorbed on Cu(111) turned out to be unstable. This structure is converted to the planar form after structural relaxation. In contrast, larger CNTs are metastable on Cu(111). They maintain the tubular geometry upon the structural optimization. Interestingly, being unstable in the freestanding state, the AC-CNT with $d = 0.4$ nm is stabilized on Cu(111).

Then, we considered possible intermediate states of the transformation of CNT to GNR on Cu(111). The planar GNR state, which corresponds to the fully opened CNT, is energetically more favorable than the partially opened CNT states (S1 and S2 in Figure 3). Figure 3 shows calculated adsorption energies E_{ad} of different configurations. It can be seen that the energy gain from the transformation of the ZZ-type CNT to GNR is more significant than that of the AC-type CNT.

According to earlier calculations, the edge formation energies of GNR are in a range from 0.39 to 0.65 eV/Å for ZZ-GNR and from 0.7 to 0.74 eV for AC-GNR [44–47]. That is, the formation of the ZZ-type edges is preferable to that of the AC-type ones due to more efficient saturation of the dangling bonds of the edge carbon atoms [44]. In contrast, in the freestanding state, the AC-GNRs are more favorable than the ZZ-GNRs [44]. This explains the smaller energy gain observed for the opening of AC-CNTs on Cu(111) compared to ZZ-CNTs.

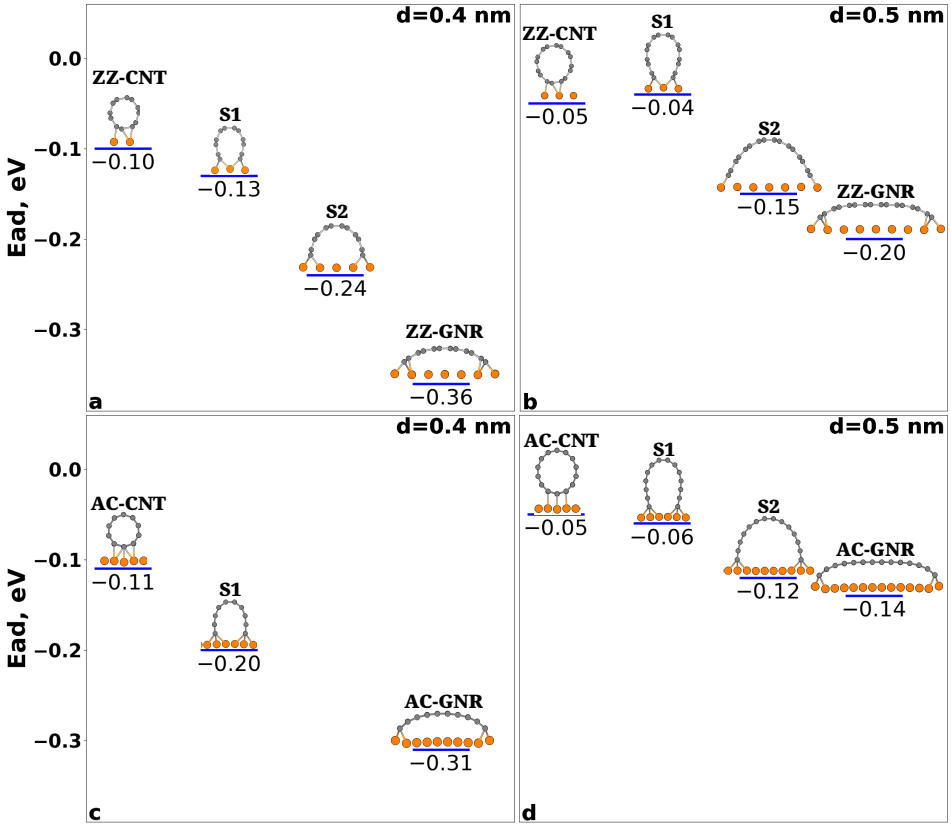

Figure 3. The adsorption E_{ad} energy per atom of the ZZ (**top**) and AC (**bottom**) CNTs on Cu(111). The CNT diameter d is 0.4 nm (**a**,**c**) and 0.5 nm (**b**,**d**).

With the increasing diameter of CNTs, the difference between energies of the adsorbed CNTs and GNRs decreases. For example, for the smallest AC-CNT considered in the present work ($d = 0.4$ nm), the adsorption energies of the CNT and GNR E_{ad} are -0.11 eV and -0.31 eV, respectively, whereas for the largest AC-CNT ($d = 0.7$ nm) the respective adsorption energies are -0.04 eV and -0.08 eV (see Table 2). The decreasing curvature of CNTs can explain such a behavior.

Table 2. The adsorption energy E_{ad} per atom of the adsorbed carbon structure on Cu(111). S1 and S2 are the possible intermediate states of the transformation of CNT to GNR on Cu(111).

d, nm	Type	E_{ad}, eV			
		CNT	S1	S2	GNR
0.4	AC	−0.11	−0.20		−0.31
	ZZ	−0.10	−0.13	−0.24	−0.36
0.5	AC	−0.05	−0.06	−0.12	−0.14
	ZZ	−0.05	−0.04	−0.15	−0.20
0.7	AC	−0.04	−0.02	−0.05	−0.08

It should be noted that our DFT calculations were performed at 0 K. At elevated temperatures atomic vibrations may lead to slight changes in adsorption geometry or interaction energies. However, we believe that the fundamental trends observed in DFT calculations, such as the relative stability of different adsorption configurations, which was the focus of our study, remain consistent at elevated temperatures.

4. Conclusions

In summary, DFT calculations show that the tubular form of carbon on Cu(111) is energetically less favorable than the planar graphene nanoribon form. The increasing diameter of CNT leads to a decreasing energy difference between the tubular and planar states due to the decreasing curvature of CNTs. The energy gain from the transformation from CNT to GNR is more significant for the ZZ-type structure than for the AC-type one. Therefore, one may expect easier opening of ZZ-CNT to ZZ-GNR on Cu(111) than in the case of AC-CNT due to a higher driving force.

Supplementary Materials: The following supporting information can be downloaded at: https://www.mdpi.com/article/10.3390/surfaces7040069/s1, Figure S1: The optimized geometry of the zigzag (top) and armchair (bottom) CNTs adsorbed on Cu(111). The dashed line indicates the unit cell used in the calculations; Figure S2: The optimized geometry of the zigzag (top) and armchair (bottom) CNTs adsorbed on Cu(111). The dashed line indicates the unit cell used in the calculations; Figure S3: Optimized geometries of the zigzag carbon nanotube transforming to the graphene nanoribbon on Cu(111).; Figure S4: Optimized geometries of the armchair carbon nanotube transforming to the graphene nanoribbon on Cu(111). Relaxed geometries of all structures are reported in the paper.

Author Contributions: Conceptualization, S.N.F.; methodology, A.A. and S.N.F.; validation, A.A.; formal analysis, A.A.; investigation, A.A. and S.N.F.; writing—original draft preparation, A.A.; writing—review and editing, A.A. and S.N.F.; visualization, A.A.; supervision, S.N.F.; project administration, S.N.F.; and funding acquisition, S.N.F. All authors have read and agreed to the published version of the manuscript.

Funding: The research was carried out with the support of a grant from the Government of the Russian Federation (Agreement No. 075-15-2024-667 of 23 August 2024).

Data Availability Statement: The raw data supporting the conclusions of this article will be made available by the authors on request.

Conflicts of Interest: The authors declare no conflicts of interest.

References

1. Novoselov, K.S.; Geim, A.K.; Morozov, S.V.; Jiang, D.; Katsnelson, M.I.; Grigorieva, I.V.; Dubonos, S.V.; Firsov, A.A. Two-dimensional gas of massless Dirac fermions in graphene. *Nature* **2005**, *438*, 197–200. [CrossRef] [PubMed]
2. Novoselov, K.S.; Jiang, Z.; Zhang, Y.; Morozov, S.; Stormer, H.; Zeitler, U.; Maan, J.C.; Boebinger, G.S.; Kim, P.; Geim, A.K. Room-temperature quantum Hall effect in graphene. *Science* **2007**, *315*, 1379–1389. [CrossRef] [PubMed]
3. Lee, C.; Wei, X.; Kysar, J.W.; Hone, J. Measurement of the elastic properties and intrinsic strength of monolayer graphene. *Science* **2008**, *321*, 385–388. [CrossRef] [PubMed]
4. Colonna, F.; Los, J.H.; Fasolino, A.; Meijer, E.J. Properties of graphite at melting from multilayer thermodynamic integration. *Phys. Rev.* **2009**, *B80*, 134103. [CrossRef]
5. Neto, A.H.C.; Guinea, F.; Peres, N.M.R.; Novoselov, K.S.; Geim, A.K. The electronic properties of graphene. *Rev. Mod. Phys.* **2009**, *81*, 109. [CrossRef]
6. Chae, S.H.; Lee, Y.H. Carbon nanotubes and graphene towards soft electronics. *Nano Converg.* **2014**, *1*, 15. [CrossRef]
7. Ouyang, J. Applications of carbon nanotubes and graphene for third-generation solar cells and fuel cells. *Nano Mater. Sci.* **2019**, *1*, 77–90. [CrossRef]
8. Hsu, C.Y.; Rheima, A.M.; Mohammed, M.S.; Kadhim, M.M.; Mohammed, S.H.; Abbas, F.H.; Abed, Z.T.; Mahdi, Z.H.; Abbas, Z.S.; Hachim, S.H.; et al. Mahmoud, E. Kianfar, Application of Carbon Nanotubes and Graphene-Based Nanoadsorbents in Water Treatment. *BioNanoScience* **2023**, *13*, 1418–1436. [CrossRef]
9. Yuan, W.; Cheng, Z.Y.L.; Wu, H.; Zheng, L.; Zhao, D. The applications of carbon nanotubes and graphene in advanced rechargeable lithium batteries. *J. Mater. Chem. A* **2016**, *4*, 8932–8951. [CrossRef]
10. Silva, A.A.; Pinheiro, R.A.; Rodrigues, A.C.; Baldan, M.R.; Trava-Airoldi, V.J.; Corat, E.J. Graphene sheets produced by carbon nanotubes unzipping and their performance as supercapacitor. *Appl. Surf. Sci.* **2018**, *446*, 201–208. [CrossRef]
11. Warbinek, J.; Leimbach, D.; Lu, D.; Wendt, K.; Pegg, D.J.; Yurgens, A.; Hanstorp, D.; Welander, J. A graphene-based neutral particle detector. *Appl. Phys. Lett.* **2019**, *114*, 061902. [CrossRef]
12. Wang, S.Y. Graphene-based detectors for directional dark matter detection. *Eur. Phys. J. C* **2019**, *79*, 561. [CrossRef]
13. Das, A.; Jang, J.; Min, H. Sub-MeV dark matter detection with bilayer graphene. *Phys. Rev. D* **2024**, *110*, 043020. [CrossRef]
14. Radsar, T.; Khalesi, H.; Ghods, V. Graphene nanoribbon field effect transistors analysis and applications. *Superlattices Microstruct.* **2024**, *153*, 106869. [CrossRef]

15. Rashid, M.H.; Koel, A.; Rang, T. Simulations of Graphene Nanoribbon Field Effect Transistor for the Detection of Propane and Butane Gases: A First Principles Study. *Nanomaterials* **2022**, *10*, 98. [CrossRef]
16. Owens, F.J. Electronic and magnetic properties of armchair and zigzag graphene nanoribbons. *J. Chem. Phys.* **2008**, *128*, 194701. [CrossRef]
17. Son, Y.-W.; Cohen, M.L.; Louie, S.G. Energy Gaps in Graphene Nanoribbons. *Phys. Rev. Lett.* **2006**, *97*, 216803. [CrossRef]
18. Li, G.; Guest, J.R.; Guisinger, N.P. Epitaxial graphene on Cu(111). *Nano Lett.* **2010**, *10*, 3512–3516. [CrossRef]
19. Li, X.; Cai, W.; An, J.; Kim, S.; Nah, J.; Yang, D.; Piner, R.; Velamakanni, A.; Jung, I.; Tutuc, E.; Banerjee, S.K.; Colombo, L.; Ruoff, R.S. Large-area synthesis of high-quality and uniform graphene films on copper foils. *Science* **2009**, *324*, 1312–1314. [CrossRef]
20. Mclellan, R.B. The solubility of carbon in solid gold, copper, and silver. *Scr. Metall.* **1969**, *3*, 389–391. [CrossRef]
21. Ishihara, M.; Koga, Y.; Kim, J.; Tsugawa, K.; Hasegawa, M. Direct evidence of advantage of Cu(111) for graphene synthesis by using Raman mapping and electron backscatter diffraction. *Mat. Let.* **2011**, *65*, 2864–2867. [CrossRef]
22. Lyding, J.; Wood, J.; Pop, E. Growing better graphene by finding the best copper surface. *SPIE Newsroom* **2012**, *10*, 004110. [CrossRef]
23. Wood, J.D.; Schmucker, S.W.; Lyons, A.S.; Pop, E.; Lyding, J.W. Effects of Polycrystalline Cu Substrate on Graphene Growth by Chemical Vapor Deposition. *Nano Lett.* **2011**, *11*, 4547–4554. [CrossRef] [PubMed]
24. Kosynkin, D.V.; Higginbotham, A.L.; Sinitskii, A.; Lomeda, J.R.; Dimiev, A.; Price, B.K.; Tour, J.M. Longitudinal unzipping of carbon nanotubes to form graphene nanoribbons. *Nature* **2009**, *458*, 872–876. [CrossRef]
25. Salah, L.S.; Ouslimani, N.; Bousba, D.; Huynen, I.; Danlée, Y.; Aksas, H. Carbon Nanotubes (CNTs) from Synthesis to Functionalized (CNTs) Using Conventional and New Chemical Approaches. *J. Nanomater.* **2021**, *2021*, 4972770. [CrossRef]
26. Saini, D. Synthesis and functionalization of graphene and application in electrochemical biosensing. *Nanotechnol. Rev.* **2016**, *5*, 393–416. [CrossRef]
27. Khalil, I.; Julkapli, N.M.; Yehye, W.A.; Basirun, W.J.; Bhargava, S.K. Graphene–Gold Nanoparticles Hybrid—Synthesis, Functionalization, and Application in a Electrochemical and Surface-Enhanced Raman Scattering Biosensor. *Materials* **2016**, *9*, 406. [CrossRef]
28. Shinde, D.B.; Debgupta, J.; Kushwaha, A.; Aslam, M.; Pillai, V.K. Electrochemical Unzipping of Multi-walled Carbon Nanotubes for Facile Synthesis of High-Quality Graphene Nanoribbons. *J. Am. Chem. Soc.* **2011**, *133*, 4168. [CrossRef]
29. Kim, K.; Sussman, A.; Zettl, A. Graphene Nanoribbons Obtained by Electrically Unwrapping Carbon Nanotubes. *ACS Nano* **2010**, *4*, 1362. [CrossRef]
30. Jiao, L.; Wang, X.; Diankov, G.; Wang, H.; Dai, H. Facile synthesis of high-quality graphene nanoribbons. *Nat. Nanotechnol.* **2010**, *5*, 321–325. [CrossRef]
31. Wang, J.; Ma, L.; Yuan, Q.; Zhu, L.; Ding, F. Transition-Metal-Catalyzed Unzipping of Single-Walled Carbon Nanotubes into Narrow Graphene Nanoribbons at Low Temperature. *Angew. Chem. Int. Ed.* **2011**, *50*, 8041–8045. [CrossRef] [PubMed]
32. Tiwary, C.S.; Javvaji, B.; Kumar, C.; Mahapatra, D.R.; Ozden, S.; Ajayan, P.M.; Chattopadhyay, K. Chemical-free graphene by unzipping carbon nanotubes using cryo-milling. *Carbon* **2015**, *89*, 217–224. [CrossRef]
33. Dong, W.; Li, X.; Lu, S.; Li, J.; Wang, Y.; Zhong, M.; Dong, X.; Xu, Z.; Shen, Q.; Gao, S.; et al. Unzipping Carbon Nanotubes to Sub-5-nm Graphene Nanoribbons on Cu(111) by Surface Catalysis. *Small* **2024**, *20*, 2308430. [CrossRef]
34. Goto, Y.; Ando, S.; Kakugawa, K.; Takahara, S.; Yamada, T.K. Unzipping Process of Wet Carbon Nanotubes Adsorbed on Cu(111) in Ultra-High Vacuum: An STM/STS study. *Vac. Surf. Sci.* **2021**, *64*, 40–46. [CrossRef]
35. Lu, J.; Yeo, P.S.E.; Gan, C.K.; Loh, W.P.K.P. Transforming C60 molecules into graphene quantum dots. *Nat. Nanotechnol.* **2011**, *6*, 247–252. [CrossRef] [PubMed]
36. Tatti, R.; Aversa, L.; Verucchi, R.; Cavaliere, E.; Garberoglio, G.; Pugno, N.M.; Speranza, G.; Taioli, S. Synthesis of single layer graphene on Cu(111) by C60 supersonic molecular beam epitaxy. *RSC Adv.* **2016**, *6*, 37982–37993. [CrossRef]
37. Blum, V.; Gehrke, R.; Hanke, F.; Havu, P.; Havu, V.; Ren, X.; Reuter, K.; Scheffler, M. Ab Initio Molecular Simulations with Numeric Atom-Centered Orbitals. *Comput. Phys. Commun.* **2009**, *180*, 2175–2196. [CrossRef]
38. Perdew, J.P.; Burke, K.; Ernzerhof, M. Generalized Gradient Approximation Made Simple. *Phys. Rev. Lett.* **1996**, *77*, 3865–3868. [CrossRef]
39. Tkatchenko, A.; Scheffler, M. Accurate Molecular Van Der Waals Interactions from Ground-State Electron Density and Free-Atom Reference Data. *Phys. Rev. Lett.* **2009**, *102*, 073005. [CrossRef]
40. Ruiz, V.G.; Liu, W.; Tkatchenko, A. Density-functional theory with screened van der Waals interactions applied to atomic and molecular adsorbates on close-packed and non-close-packed surfaces. *Phys. Rev. B* **2016**, *93*, 035118. [CrossRef]
41. Momma, K.; Izumi, F. VESTA 3 for three-dimensional visualization of crystal, volumetric and morphology data. *J. Appl. Crystallogr.* **2011**, *44*, 1272–1276. [CrossRef]
42. Straimanis, M.E.; Yu, L.S. Lattice parameters, densities, expansion coefficients and perfection of structure of Cu and of Cu-In phase. *Acta Cryst.* **1969**, *A25*, 676–682. [CrossRef]
43. Sun, W.; Ceder, G. Efficient creation and convergence of surface slabs. *Surf. Sci.* **2013**, *617*, 53–59. [CrossRef]
44. Artyukhov, V.I.; Liu, Y.Y.; Yakobson, B.I. Equilibrium at the edge and atomistic mechanisms of graphene growth. *Proc. Natl. Acad. Sci. USA* **2012**, *109*, 15136–15140. [CrossRef] [PubMed]
45. Gao, J.; Zhao, J.; Ding, F. Transition Metal Surface Passivation Induced Graphene Edge Reconstruction. *J. Am. Chem. Soc.* **2012**, *134*, 6204–6209. [CrossRef]

46. Shu, H.; Chen, X.; Tao, X.; Ding, F. Edge Structural Stability and Kinetics of Graphene Chemical Vapor Deposition Growth. *ACS Nano* **2012**, *6*, 3243–3250. [CrossRef]
47. Shu, H.; Chen, X.; Ding, F. The Edge Termination Controlled Kinetics in Graphene Chemical Vapor Deposition Growth. *Chem. Sci.* **2014**, *5*, 4639–4645. [CrossRef]